

Geophysical Research Letters[®]

RESEARCH LETTER

10.1029/2021GL093069

Key Points:

- Model results show that sea ice drift leads to increases or decreases in ice area depending on season, drift velocity, and climate forcing
- Equatorward ice drift during seasonal retreat mostly causes ice area loss, whereas during advance it often causes increases in area
- Equatorward ice drift consistently causes ice volume loss, with higher velocities leading to more pronounced volume loss

Supporting Information:

Supporting Information may be found in the online version of this article.

Correspondence to:

T. J. W. Wagner,
till.wagner@wisc.edu




Citation:

Wagner, T. J. W., Eisenman, I., & Mason, H. C. (2021). How sea ice drift influences sea ice area and volume. *Geophysical Research Letters*, 48, e2021GL093069. <https://doi.org/10.1029/2021GL093069>

Received 20 FEB 2021

Accepted 15 SEP 2021

How Sea Ice Drift Influences Sea Ice Area and Volume

T. J. W. Wagner^{1,2} , I. Eisenman³ , and H. C. Mason^{1,4} 

¹Department of Physics and Physical Oceanography, University of North Carolina Wilmington, Wilmington, NC, USA,

²Department of Atmospheric and Oceanic Sciences, University of Wisconsin-Madison, Madison, WI, USA, ³Scripps Institution of Oceanography, University of California San Diego, La Jolla, CA, USA, ⁴Courant Institute of Mathematical Sciences, New York University, New York, NY, USA

Abstract Equatorward sea ice drift can have competing impacts on the sea ice cover. On one hand, as ice reaches warmer waters it will be subject to faster melt. On the other hand, the ice near the pole will thin, causing faster ice growth when air temperatures are below freezing. This prompts the fundamental question whether equatorward ice motion increases or decreases ice area and volume? We investigate this using an idealized climate model with a representation of sea ice thermodynamic processes and specified sea ice drift. We find that equatorward ice drift leads to consistent loss of ice volume. The impact of ice motion on ice area depends on seasonal factors and the background climate: When there is enough ice, equatorward ice motion slightly expands ice area. For thinner ice, however, motion during the melt season can create polynyas and cause substantial ice loss that persists throughout the year.

Plain Language Summary If sea ice is pushed to lower latitudes by winds and currents, do sea ice area and volume increase or decrease? We investigate this question using an idealized climate model. We find that sea ice *volume* is always decreased by equatorward motion of sea ice: The ice melts in warmer waters faster than it can refreeze near the pole. However, the *area* covered by sea ice can increase through equatorward motion (in particular in cool climates and when motion occurs in the winter growth season) or decrease (especially in warmer climates or when motion occurs during the summer melt season).

1. Introduction

The areal cover of sea ice in the polar regions is determined by thermodynamic ice melt and growth on the one hand and dynamic ice motion and hence volume redistribution on the other hand. The dynamic processes are highly complex and include ice drift and the opening of leads and polynyas, as well as rafting of ice floes and the formation of pressure ridges. The complexity of these processes presents a formidable challenge to accurately modeling the evolution of the sea ice cover, and even state-of-the-art climate models that include sophisticated representations of sea ice rheology (e.g., Hunke & Dukowicz, 1997) often struggle to reproduce observed sea ice evolution and trends (e.g., Pörtner et al., 2019, Ch. 3).

For example, despite global warming, Antarctic sea ice expanded in the annual mean during 1979–2013 at a rate of 2 million km² yr⁻¹ (Fetterer et al., 2002). However, in simulations from the suite of comprehensive global climate models (GCMs) carried out by international modeling groups for the Coupled Model Inter-comparison Project phase 5 (CMIP5) (Taylor et al., 2011), the vast majority of runs have retreating Antarctic sea ice over this period (e.g., 107 out of 118 runs analyzed by Rosenblum & Eisenman, 2017) in contrast with the observations. Sea ice motion has emerged in recent years as one of the leading proposed mechanisms to explain this apparent paradox (Blanchard-Wrigglesworth et al., 2021; Holland & Kwok, 2012; Sun & Eisenman, 2021; Turner et al., 2009, 2016). Yet, the fundamental processes by which sea ice motion impacts the sea ice cover remain poorly understood, and open questions persist as to the role of ice motion in phenomena including the observed multi-decadal Antarctic sea ice expansion (e.g., Holland, 2014).

Sea ice drift also plays an important role in setting the areal cover and ice thickness distribution in the Arctic Ocean. As the summer sea ice in the Arctic continues to retreat under global warming, it is becoming less confined by its coastlines. This, in combination with a strengthening of winds (Smedsrud et al., 2017), may have led to the observed speed-up of sea ice drift in recent decades (Spren et al., 2011). The more vigorous drift may explain why the export of ice area through Fram Strait has been increasing (Smedsrud

et al., 2017). Volume export through Fram Strait, by contrast, has decreased due to the substantial overall thinning of the ice cover (Spreen et al., 2020). These observations highlight how sea ice drift and thermodynamic processes interact to influence trends in ice area and volume.

While the particular Arctic and Antarctic sea ice changes provide the underlying motivation for this study, we do not aim to replicate any specific geographic conditions. Instead, here we focus on the fundamental processes by which ice motion determines the seasonal cycle of sea ice. We do so using an idealized model of the global climate and sea ice. We note that the idealized model developed here is designed to build understanding, rather than to simulate the details of the climate system as in a comprehensive climate modeling approach (Held, 2005). Specifically, we aim to address the question: *Does equatorward sea ice motion increase or decrease sea ice area and volume?* The answer to this question is not intuitively straightforward, because equatorward drift of sea ice can have competing impacts on sea ice area and volume. On the one hand, divergence in the ice velocity field spreads the ice cover, thereby increasing the total ice extent while thinning the ice. Hence divergence in the velocity field or equatorward ice motion has been suggested to cause ice expansion, as mentioned above (e.g., Holland & Kwok, 2012; Turner et al., 2009, 2016). Note that since thin ice grows faster than thick ice (e.g., Bitz & Roe, 2004; Eisenman & Wettlaufer, 2009), the volume of the ice may also be expected to increase. On the other hand, divergence in the sea ice velocity has also been suggested as an explanation for sea ice contraction, because sea ice is removed from the polar region. This rationale has been applied mainly in the Arctic, where studies have ascribed ice loss to equatorward ice motion through Fram Strait (e.g., Ogi & Rigor, 2013; Ogi et al., 2010; Rigor & Wallace, 2004; Rigor et al., 2002; Wettstein & Deser, 2014).

Factors we will focus on in this study are the drift speed, the time of year during which the motion occurs, and the background climate.

2. Idealized Model of Global Climate and Sea Ice

The model we use is adapted from Wagner and Eisenman (2015) (hereafter WE15), which is based on the longstanding framework of diffusive energy balance models (Budyko, 1969; North et al., 1981; Sellers, 1969), with the addition of a seasonal cycle, an aquaplanet slab ocean mixed layer, and a representation of sea ice thermodynamic processes based on previous single column sea ice models (Eisenman & Wettlaufer, 2009; Maykut & Untersteiner, 1971; Thorndike, 1992). The model simulates the time evolution of the zonally averaged surface temperature and sea ice thickness as functions of latitude.

The state of the system is described by the surface enthalpy, $E(t, x)$, which contains information about both surface temperature and ice thickness and varies with time and spatial coordinate $x \equiv \sin \theta$, with θ the latitude. Specifically, in ice-free regions $E = c_w T$ with c_w the heat capacity of the ocean mixed layer and T the surface temperature measured in terms of the departure from the freezing point. Hence $E \geq 0$ in all ice-free regions. When the ocean mixed layer cools until it reaches the freezing point ($E = 0$), any additional heat loss causes sea ice growth with the ocean mixed layer remaining at the freezing point. In this case, $E = -L_f h$, with sea ice thickness h and sea ice latent heat of fusion L_f . Hence $E < 0$ indicates ice-covered regions, and the sea ice areal extent is the size of the region with $E < 0$. The surface temperature T in regions with sea ice is determined diagnostically based on a balance of vertical energy fluxes (see details in Supporting Information Text S1).

The model can be summarized by a single partial differential equation expressing that E evolves according to the zonally averaged net energy flux into a column of the climate system:

$$\frac{\partial E}{\partial t} = \underbrace{aS}_{\text{solar}} - \underbrace{(A + BT)}_{\text{OLR}} + \underbrace{D\nabla_x^2 T}_{\text{transport}} + \underbrace{F_b}_{\text{ocean heating}} + \underbrace{F}_{\text{climate forcing}} + \underbrace{MH(-E)}_{\text{ice motion}}. \quad (1)$$

The terms on the right-hand side represent the seasonally varying incident solar radiation at the top of the atmosphere $S(t, x)$ scaled by the top-of-atmosphere coalbedo $a(x, E)$ which depends on the presence of ice as well as the solar zenith angle; the outgoing longwave radiation (OLR) which is represented as a linear function of the surface temperature, with A and B constants (Budyko, 1969; Koll & Cronin, 2018; North

et al., 1981); meridional heat transport in the atmosphere and ocean, which is represented as diffusion of the surface temperature, $D\nabla_x^2 T$ (Budyko, 1969); upward heat flux from the ocean below, F_b ; and imposed climate forcing F , which can be varied to represent changing greenhouse gas levels. We assume symmetry between the two hemispheres, which allows us to run the simulations using a domain that represents a single hemisphere, as in WE15. The model parameter values and model equations are given in the Supporting Information S1, and further details of the model formulation can be found in WE15.

In the present study, we modify the model of WE15 by adding specified horizontal ice motion, which is represented by the final term in Equation 1. The ice motion takes the advective form $M \equiv \nabla \cdot (E\mathbf{u})$. In spherical coordinates, with E varying only in x and purely meridional velocity $\mathbf{u} = v\hat{x}$ with constant v (given in standard dimensions of length per time) and \hat{x} the northward pointing unit vector, this takes the form

$$M = \frac{v}{r} \frac{\partial}{\partial x} \left(E \sqrt{1 - x^2} \right), \quad (2)$$

with r the radius of Earth. This represents 1-D meridional advection of ice, with the $\sqrt{1 - x^2}$ term accounting for the convergence of meridians. Here positive values of v indicate equatorward motion. In Equation 1, this term is multiplied by the Heaviside function \mathcal{H} so that only ice thickness is advected (i.e., advection occurs only where $E < 0$).

Sea ice resists deformation in the real world, which limits convergence in ice velocity fields especially where the ice is thick. Here we crudely account for this by turning off advection wherever it would lead to ice growth when the ice thickness $h > 4$ m, analogous to sea ice rheology “stoppage” schemes used in early GCMs (e.g., Flato, 2004). In our framework, this only occurs in simulations with ice motion toward the pole. Since we primarily focus on equatorward ice motion, the 4 m threshold does not influence most of the results presented below.

The idealized nature of the model allows a physically intuitive framework for investigating the impact of dynamic ice motion on thermodynamic ice growth and melt. However, it limits the ability to directly compare results with the observed seasonal cycle of the ice cover in the Arctic (which is influenced by coastlines among other factors that are not represented here) and the Antarctic (which is influenced by the Antarctic Circumpolar Current among other factors that are not represented here) (Bitz et al., 2005).

Nonetheless, we use a broadly qualitative comparison with observations to validate the model with the added ice motion scheme. Using satellite-derived monthly mean ice velocity data (Tschudi et al., 2019), we spatially average the meridional velocity over a region off the coast of Antarctica’s Dronning Maud Land (Figure S1b) and then compute the 1995–2015 mean velocity seasonal cycle (Figure S2b inset). This region is chosen because it features predominantly meridional ice motion throughout the year. We force the model with this observationally based estimate of $v(t)$, placing an idealized landmass at $\theta > 70^\circ$ in these simulations in order to better compare with observations but otherwise leaving the model parameters unchanged. For simplicity, the Antarctic landmass is represented here as sea ice with thickness fixed at $h = 100$ m, which ensures that the heat flux through the sea ice is negligible and the surface temperature, T , is determined by the surface fluxes only, somewhat resembling the energy balance for the surface of an ice sheet. The simulation results, averaged zonally over the same region and averaged over the same time period (Figure S3a), are compared with the observationally based Antarctic ice thickness estimate from the GIOMAS product (Zhang & Rothrock, 2003) (Figures S1a and S2a). The simulations show broad qualitative agreement with the observations. Using instead a simulation with $v = 0$ (Figure S3b) leads to less agreement with the observations. In particular, for the simulations without ice motion, the ice is thickest at the highest latitudes, whereas in the simulations with ice motion the thickest ice is several degrees further equatorward, as in the observations.

For the main set of simulations, we eschew the added complexity associated with having landmass at $\theta > 70^\circ$, such that the model represents an aquaplanet. As discussed in the introduction, the purpose of this study is to probe the underlying dynamics that link sea ice motion to changes in ice area and volume, rather than replicate particular geographic conditions. Questions regarding the role of certain landmass distributions or wind patterns are more fittingly tackled using comprehensive modeling approaches, such as was recently done, for example, by Sun and Eisenman (2021).

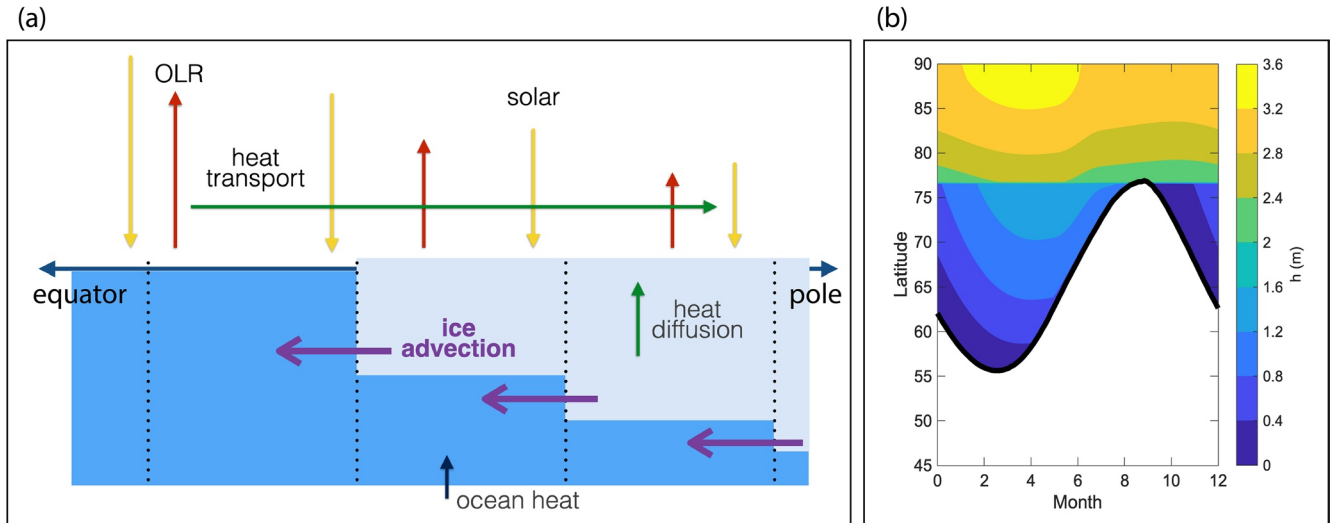


Figure 1. Model setup and default simulation results. (a) Schematic of the energy fluxes represented in the model: net solar radiation (yellow), outgoing longwave radiation (red), ocean heating (blue), meridional heat transport (green), and vertical heat diffusion within the sea ice (green). The sea ice in each gridbox is moved equatorward at a prescribed velocity (purple arrows). The model simulates the evolution of the water temperature or sea ice thickness at each gridbox. (b) Seasonal cycle of sea ice thickness (contours) in the default simulation that includes no ice motion ($v = 0$) and no climate forcing ($F = 0$). Here the horizontal axis spans one year, and the vertical coordinate spans from 45° latitude to the pole. The black line marks the ice edge ($E = 0$).

In what follows, we consider the impact of sea ice drift on the ice cover for different background climates, with climate forcing ranging from $F = 0$ to 6.5 W m^{-2} . Here, $F = 0$ corresponds to the current climate, with a sea ice seasonal cycle that is qualitatively similar to the present-day Arctic sea ice cover, and $F = 4 \text{ W m}^{-2}$ is the level of climate forcing at which the pole first becomes seasonally ice-free when there is no ice motion. We consider ice drift speeds in the range $v = 0$ to 25 cm s^{-1} , with the latter representing the approximate upper limit of sustained meridional drift speeds in the observations (Tschudi et al., 2019).

To probe the role that seasonality plays in how sea ice motion impacts ice area and volume, we perform simulations that move ice (*i*) continuously throughout the year; (*ii*) for six months in the advancing or the retreating periods of the year, which we refer to as “winter” and “summer” motion; and (*iii*) in a single month. In other words, ice drift speed v is set to take a spatially and temporally constant non-zero value in each simulation during (*i*) twelve, (*ii*) six, or (*iii*) one month each year and set to zero for all other months. The model is run for 60 years, and the results during the final year are plotted. Note that in longer simulations (to test the spinup time), the change in annual-mean ice thickness at the pole between year 60 and year 120 was found to be $< \%$, and the change in the annual-mean ice edge was $< 0.1\%$.

3. Results

The seasonal cycle simulated with the default configuration with no motion ($v = 0$) and no climate forcing ($F = 0$) is shown in Figure 1b. The perennial sea ice cover extends to a latitude of 75° ($x = 0.97$) with ice thickness of $2.5 - 3.2 \text{ m}$. The seasonal ice cover extends to a minimum latitude of 55° ($x = 0.82$) in the winter (with ice thickness $< 1.5 \text{ m}$). This approximately matches the zonal mean thickness (Kwok & Cunningham, 2015) and ice edge latitude (Eisenman et al., 2011) of the modern-day summer minimum and winter maximum Arctic sea ice cover.

The impact of different drift speeds and drift seasons are illustrated in Figure 2 for the simulated default climate with $F = 0$. The top row shows the ice thickness for equatorward drift of $v = 3 \text{ cm s}^{-1}$, with the different panels representing motion in winter only, summer only, or throughout the year. We find that for this relatively slow drift, ice area is nearly unchanged, regardless of the drift season. Summer motion leads to a small increase in ice area near the time of the summer minimum, whereas year-round motion leads to a small decrease in ice area near the summer minimum due to loss of ice cover at the pole. However, for all drift periods the ice thickness distribution is notably altered compared to the no-motion run of Figure 1b.

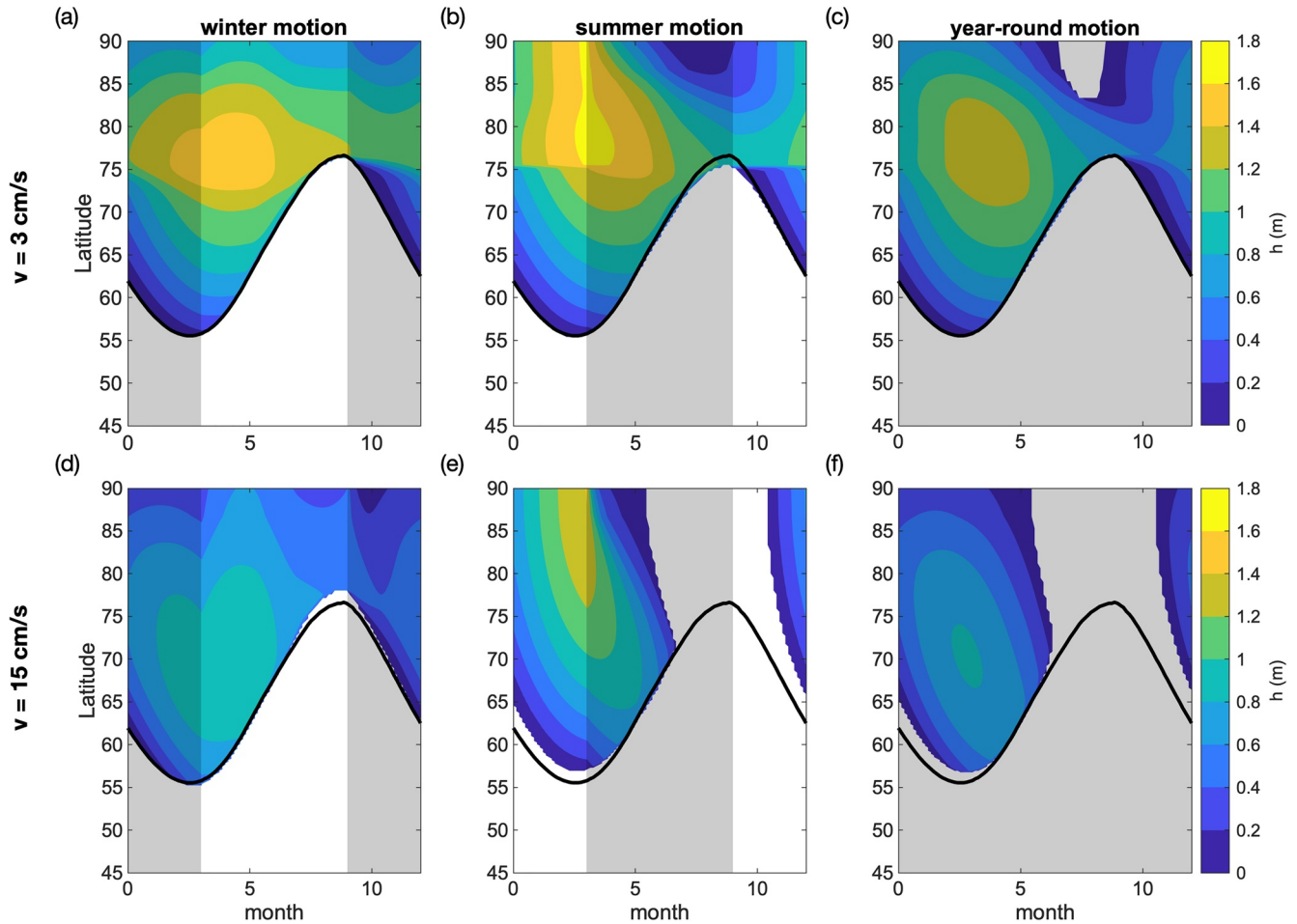


Figure 2. Seasonal cycle of sea ice thickness, as in Figure 1b but with prescribed equatorward drift of $v = 3 \text{ cm s}^{-1}$ (top row) and $v = 15 \text{ cm s}^{-1}$ (bottom row) during some or all of the year. The gray shaded regions in each panel depict the periods in which there is ice motion: the left column has motion only during the six months of ice advance (“winter”), the middle column has motion only during the six months of ice retreat (“summer”), and the right column has motion throughout the year. The black line is repeated from Figure 1b, indicating the ice edge in the control simulation with no ice motion. As in Figure 1b, here the climate forcing is $F = 0$ and all other parameters are as given in Table S1. Note that the ice thickness color scale spans half the range of that for Figure 1b.

The thickest ice is found at $\sim 80^\circ$ latitude, rather than at the pole, and the ice thickness in the high latitudes is approximately halved (maximum thickness of $h = 1.6 \text{ m}$, compared to 3.2 m in the no-motion run). Furthermore, the step in thickness between perennial and seasonal ice is visibly smoothed out when there is ice motion during any part of the year.

The bottom row of Figure 2 illustrates that both ice area and ice volume are substantially more impacted as drift speeds are increased. Here, $v = 15 \text{ cm s}^{-1}$, which is faster than $>95\%$ of observed meridional drift speeds (Tschudi et al., 2019). In this case, ice motion during the period of ice retreat (Figure 2e) leads to loss of ice at the pole (i.e., the opening of a polynya) in early June and complete loss of all ice by late June. The associated increase in the absorption of sunlight results in a warmer overall climate (not shown), and the ice reduction is carried over into the next freezing period. Year-round ice drift (Figure 2f) results in areal ice loss that strikingly resembles the summer-only ice drift simulation (Figure 2e). Winter motion (Figure 2d), on the other hand, has little impact on the sea ice area even at this rapid drift speed: it leads to a slight increase in ice area around the winter maximum, and a slight decrease of ice area around the summer minimum. The decrease near the summer minimum is associated with a substantially reduced overall ice thickness.

The information in Figure 2 can be further illustrated by line plots of the seasonal cycles of sea ice area and sea ice volume, which are shown in Figure 3. Drift at $v = 3 \text{ cm s}^{-1}$ has little impact on ice area (Figure 3a),

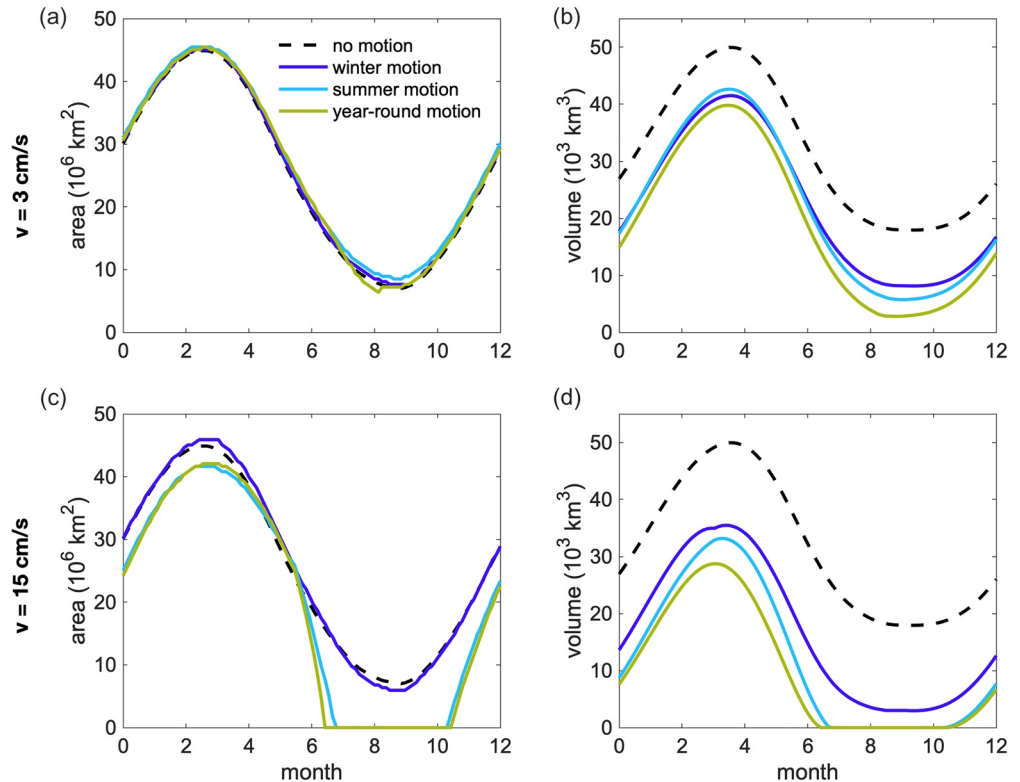


Figure 3. Seasonal cycle of sea ice area (left column) and sea ice volume (right column) for the simulations with varied ice motion plotted in Figures 1b and 2. Here there is prescribed equatorward drift of $v = 3 \text{ cm s}^{-1}$ (top row) and $v = 15 \text{ cm s}^{-1}$ (bottom row), with the no-motion case also indicated.

regardless of the season of motion. Year-round and summer motion at $v = 15 \text{ cm s}^{-1}$ result in a substantial reduction of ice area throughout the year, with complete loss from late June to early October (Figure 3c). Summer-only motion causes nearly the same reduction in ice area loss as year-round motion, and winter-only motion has little impact on the area. The change in total ice volume, on the other hand, is less dependent on the period of motion, scaling more gradually with drift speed (Figures 3b and 3d). And even though ice area loss is much more pronounced for summer-only and year-round motion than for winter motion, the loss of ice volume is almost as large for winter-only simulations as it is in the other two cases.

The results shown in Figures 2 and 3 are repeated for a warmer background climate ($F = 4 \text{ W m}^{-2}$) in Figures S4 and S5. Qualitatively, the patterns of ice area and volume loss are similar between the two background climates ($F = 0$ and $F = 4 \text{ W m}^{-2}$), with the main difference being that summers are already ice free for $F = 4 \text{ W m}^{-2}$ with no motion, so the reductions of ice area and volume due to motion are muted compared to the simulations with $F = 0$ and perennial sea ice.

To achieve a broader perspective of the impact of equatorward sea ice drift on ice area and ice volume, we perform simulations over a range of background states and drift velocities, with F varying from 0 to 6.5 W m^{-2} at 0.5 W m^{-2} increments and v varying over the full observed range of velocities, from 0 to 25 cm s^{-1} , at 1 cm s^{-1} increments. The results for ice motion during six months around summer only, six months around winter only, and throughout the full year are illustrated in Figure 4. In this figure, we show the change in annual-mean ice area and ice volume relative to the default simulation (which has $v = 0$) for each forcing. Qualitative features of the simulations remain unchanged over this broader range of values of F and v : summer motion reduces ice area almost as much as year-round motion, and it has a much more pronounced effect on sea ice area than winter motion. Figure 4 also shows that equatorward drift tends to cause the ice area to increase as long as the ice cover is perennial, whereas it always causes the ice area to decrease when the ice cover is seasonal. Ice volume, on the other hand, is always reduced by equatorward ice drift, regardless of the values of F and v or the season when ice motion occurs.

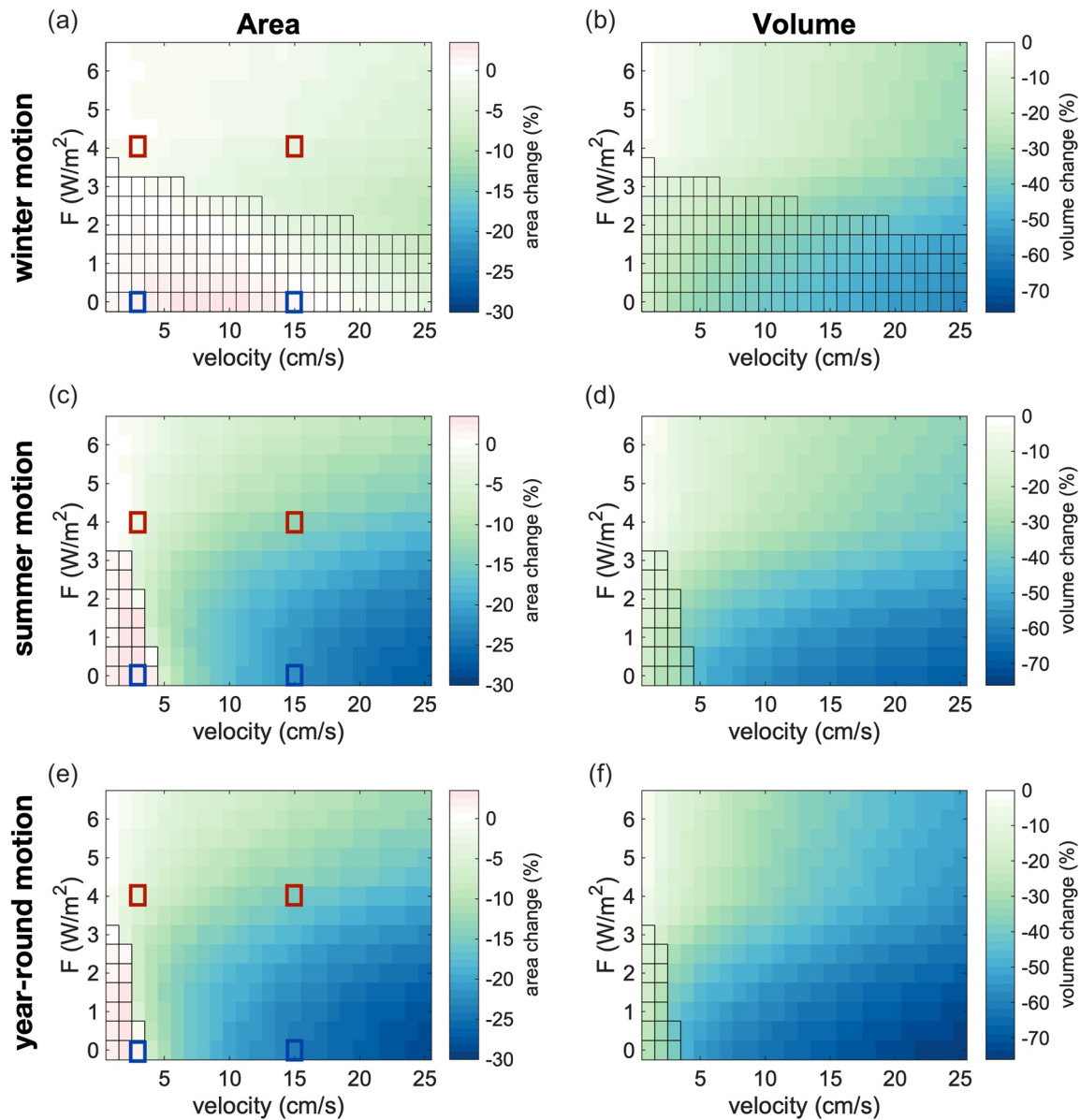


Figure 4. Annual-mean response of the sea ice cover to equatorward ice drift, for different climate forcings F (vertical axes) and equatorward drift speeds v (horizontal axes). The left column shows the percentage change in sea ice area, and the right column shows the percentage change in sea ice volume, both relative to the control simulation (which has $v = 0$) for each forcing. The top, middle, and bottom rows have winter-only motion, summer-only motion, and year-round motion, respectively. Black boxes indicate simulations with a perennial ice cover, and a seasonal ice cover occurs in the other simulations (none of the plotted simulations are ice-free throughout the year). The blue squares correspond to the simulations shown in Figure 2 and the red squares to those in Figure S4.

Further details regarding the sensitivity to the timing of ice drift are provided in Figures S6 and S7, which show simulations that have ice motion during a single month only. Figure S6 shows results equivalent to the bottom row of Figure 2. The ice area loss and ice volume loss in the case when ice motion occurs during a single month are broadly similar to the results when motion occurs during a full season, and they show that ice area is most strongly impacted by motion during May and June, which are the months with the maximum rate of seasonal ice retreat. Figure S7 shows results equivalent to Figure 4. When ice motion occurs during only a single month, it leads to a relatively modest increase in ice area in most cases. However, the ice loss associated with a seasonally ice-free pole under ice motion during May and June remains the most pronounced signal. Regarding ice volume changes, ice motion during a single month causes volume

reduction regardless of month of motion, background climate, or drift speed, similar to the case when there is motion during a full season.

4. Discussion and Conclusions

We find that equatorward ice motion can lead to seasonal expansion or contraction of the ice area: on the one hand, if there is sufficient ice to be moved, a slight expansion of the ice cover typically occurs during part of the year in response to equatorward drift. This occurs for winter-only ice motion in Figure 3, and it also occurs when there is ice motion during a single month of the winter or summer in Figure S6. On the other hand, contraction occurs if the ice is thinned sufficiently throughout the year. This contraction tends to be most pronounced around the time of the summer minimum (Figures 2d–2f).

The largest changes in ice area occur when ice motion causes the opening of a summer polynya at the pole (Figures 2e and 2f). In this case, the change in surface albedo at the pole heats the region, and the remaining ice equatorward of the polynya quickly melts away. Whether the pole becomes ice-free depends on how fast the ice is drifting and when the drift occurs. Figure 4c shows that for the default climate ($F = 0$), drift during the summer half-year at $v = 5 \text{ cm s}^{-1}$ is sufficient to cause ice-free summers. On the other hand, when the drift occurs only in the month of May (which is the month of fastest summer ice retreat), ice-free summers occur when the drift speed is at least $v = 16 \text{ cm s}^{-1}$ (Figure S7). It is notable that ice drift most readily causes seasonally ice-free conditions when the drift occurs during the time of summer ice retreat. When the drift occurs instead only during the time of winter ice advance, new ice typically grows at the pole as the ice drifts equatorward. This can be seen in Figure S7: the edge of the region with black boxes has the highest slopes in the panels with ice motion during May through July, indicating that changes in v rather than changes in F most readily cause seasonally ice-free conditions during those months.

We note that the maximum *increase* in ice area due to drift in these simulations is $\approx 3\%$, regardless of the period when the drift occurs (Figure 4). The maximum *decrease* in ice area, on the other hand, is $\approx -30\%$, which happens under cold background climates ($F \approx 0$), fast drift speeds ($v \approx 25 \text{ cm s}^{-1}$), and when drift occurs during the summer months.

Equatorward motion always causes sea ice *volume* to diminish, regardless of the background climate, drift speed, period when the drift occurs, and whether the ice cover is perennial or seasonal. This may be explained in terms of the extra ice melt due to ice drifting to warmer latitudes always being larger than the extra growth due to thinner ice at high latitudes. The volume loss is largest when drift occurs during the summer months (Figures 4 and S7), although the difference in volume loss between summer and winter motion is not as pronounced as the difference in area loss. Under default climate forcing $F = 0$, fast ice drift speeds of 25 cm s^{-1} cause an ice volume loss of $\sim 75\%$ compared with the volume when there is no motion (Figure 4f).

In summary, we find that equatorward sea ice motion leads to

1. a substantial reduction in sea ice volume regardless of background climate, drift speed, and drift season.
2. a modest increase in sea ice area during the period of ice motion as long as there is enough ice.
3. a modest increase in sea ice area year-round if the background state is cold enough and the ice is sufficiently thick for the ice cover to be maintained year-round.
4. a substantial reduction (up to complete summer loss) in sea ice area when ice drift occurs during the summer ice retreat season and when the ice cover is sufficiently thin. In this case, ice motion can cause an ice-free polynya at the pole in mid summer and completely ice-free conditions by late summer, with the ice motion causing a reduction in sea ice area for most or all of the year.

It should be emphasized that although the phase of the seasonal cycle in these figures indicate the Northern Hemisphere climate, the idealized model results presented here could just as readily be interpreted to represent the Southern Hemisphere. Considering the observed changes in Antarctic sea ice area during recent decades, the results of this study are somewhat ambiguous: they support the idea that sea ice area should increase in response to enhanced equatorward ice motion as long as the sea ice is sufficiently thick, such as in areas like the Weddell Sea where there is a substantial amount of thick perennial ice. However, around most of Antarctica, where the sea ice cover is largely seasonal, these results suggest that enhanced

equatorward ice motion would lead to a reduction of the ice area. Further work is merited to provide a more conclusive answer regarding the role of ice motion in the observed changes in Antarctic sea ice area. The results of this study provide an idealized theoretical framework to aid in the interpretation of changes in sea ice area and sea ice volume that coincide with changes in the sea ice drift field.

Data Availability Statement

Modeling code is available from the authors at <https://doi.org/10.5281/zenodo.4005793>. GIOMAS data is available at http://psc.apl.washington.edu/zhang/Global_seaice/data.html and estimated sea ice motion data is available at <https://nsidc.org/data/NSIDC-0116/>.

Acknowledgments

This study was supported by NSF OPP grant 1643445.

References

- Bitz, C. M., Holland, M. M., Hunke, E. C., & Moritz, R. E. (2005). Maintenance of the sea-ice edge. *Journal of Climate*, 18(15), 2903–2921. <https://doi.org/10.1175/jcli3428.1>
- Bitz, C. M., & Roe, G. H. (2004). A mechanism for the high rate of sea ice thinning in the Arctic Ocean. *Journal of Climate*, 17(18), 3623–3632. [https://doi.org/10.1175/1520-0442\(2004\)017<3623:amfthr>2.0.co;2](https://doi.org/10.1175/1520-0442(2004)017<3623:amfthr>2.0.co;2)
- Blanchard-Wrigglesworth, E., Roach, L. A., Donohoe, A., & Ding, Q. (2021). Impact of winds and southern ocean ssts on Antarctic sea ice trends and variability. *Journal of Climate*, 34(3), 949–965. <https://doi.org/10.1175/jcli-d-20-0386.1>
- Budyko, M. I. (1969). The effect of solar radiation variations on the climate of the Earth. *Tellus*, 21, 611–619. <https://doi.org/10.3402/tellusa.v21i5.10109>
- Eisenman, I., Schneider, T., Battisti, D. S., & Bitz, C. M. (2011). Consistent changes in the sea ice seasonal cycle in response to global warming. *Journal of Climate*, 24(20), 5325–5335. <https://doi.org/10.1175/2011JCLI4051.1>
- Eisenman, I., & Wettlaufer, J. S. (2009). Nonlinear threshold behavior during the loss of Arctic sea ice. *Proceedings of the National Academy of Sciences of the United States of America*, 106(1), 28–32. <https://doi.org/10.1073/pnas.0806887106>
- Fetterer, F., Knowles, K., Meier, W., & Savoie, M. (2002). *Sea ice index*. Boulder, CO: National Snow and Ice Data Center. Retrieved from <http://nsidc.org/data/g02135.html>
- Flato, G. M. (2004). Sea-ice modelling. In *Mass balance of the cryosphere* (pp. 367–390). Cambridge University Press. <https://doi.org/10.1017/cbo9780511535659.011>
- Held, I. M. (2005). The gap between simulation and understanding in climate modeling. *Bulletin of the American Meteorological Society*, 86(11), 1609–1614. <https://doi.org/10.1175/bams-86-11-1609>
- Holland, P. R. (2014). The seasonality of Antarctic sea ice trends. *Geophysical Research Letters*, 41(12), 4230–4237. <https://doi.org/10.1002/2014GL060172>
- Holland, P. R., & Kwok, R. (2012). Wind-driven trends in Antarctic sea-ice drift. *Nature Geoscience*, 5(12), 872–875. <https://doi.org/10.1038/NNGEO1627>
- Hunke, E. C., & Dukowicz, J. K. (1997). An elastic-viscous-plastic model for sea ice dynamics. *Journal of Physical Oceanography*, 27(9), 1849–1867. [https://doi.org/10.1175/1520-0485\(1997\)027<1849:aevpml>2.0.co;2](https://doi.org/10.1175/1520-0485(1997)027<1849:aevpml>2.0.co;2)
- Koll, D. D. B., & Cronin, T. W. (2018). Earth's outgoing longwave radiation linear due to H₂O greenhouse effect. *Proceedings of the National Academy of Sciences of the United States of America*, 115(41), 10293–10298. <https://doi.org/10.1073/pnas.1809868115>
- Kwok, R., & Cunningham, G. (2015). Variability of Arctic sea ice thickness and volume from CryoSat-2. *Philosophical Transactions of the Royal Society A: Mathematical, Physical and Engineering Sciences*, 373(2045), 20140157. <https://doi.org/10.1098/rsta.2014.0157>
- Maykut, G. A., & Untersteiner, N. (1971). Some results from a time-dependent thermodynamic model of sea ice. *Journal of Geophysical Research*, 76, 1550–1575. <https://doi.org/10.1029/jc076i006p01550>
- North, G. R., Cahalan, R. F., & Coakley, J. A., Jr. (1981). Energy balance climate models. *Reviews of Geophysics and Space Physics*, 19, 91–121. <https://doi.org/10.1029/rg019i001p00091>
- Ogi, M., & Rigor, I. G. (2013). Trends in Arctic sea ice and the role of atmospheric circulation. *Atmospheric Science Letters*, 14(2), 97–101. <https://doi.org/10.1002/asl2.423>
- Ogi, M., Yamazaki, K., & Wallace, J. M. (2010). Influence of winter and summer surface wind anomalies on summer Arctic sea ice extent. *Geophysical Research Letters*, 37, L07701. <https://doi.org/10.1029/2009GL042356>
- Pörtner, H.-O., Roberts, D. C., Masson-Delmotte, V., Zhai, P., Tignor, M., Poloczanska, E., et al. (2019). IPCC Special Report on the Ocean and Cryosphere in a Changing Climate. *IPCC Intergovernmental Panel on Climate Change: Geneva, Switzerland*, Vol. 1(3).
- Rigor, I. G., & Wallace, J. M. (2004). Variations in the age of Arctic sea-ice and summer sea-ice extent. *Geophysical Research Letters*, 31(9), L09401. <https://doi.org/10.1029/2004gl019492>
- Rigor, I. G., Wallace, J. M., & Colony, R. L. (2002). Response of sea ice to the Arctic oscillation. *Journal of Climate*, 15(18), 2648–2663. [https://doi.org/10.1175/1520-0442\(2002\)015<2648:rositt>2.0.co;2](https://doi.org/10.1175/1520-0442(2002)015<2648:rositt>2.0.co;2)
- Rosenblum, E., & Eisenman, I. (2017). Sea ice trends in climate models only accurate in runs with biased global warming. *Journal of Climate*, 30(16), 6265–6278. <https://doi.org/10.1175/jcli-d-16-0455.1>
- Sellers, W. D. (1969). A global climate model based on the energy balance of the Earth-atmosphere system. *Journal of Applied Meteorology*, 8, 392–400. [https://doi.org/10.1175/1520-0450\(1969\)008<0392:agcmbo>2.0.co;2](https://doi.org/10.1175/1520-0450(1969)008<0392:agcmbo>2.0.co;2)
- Smedsrud, L. H., Halvorsen, M. H., Stroeve, J. C., Zhang, R., & Kloster, K. (2017). Fram strait sea ice export variability and September Arctic Sea ice extent over the last 80 years. *The Cryosphere*, 11(1), 65–79. <https://doi.org/10.5194/tc-11-65-2017>
- Spreen, G., de Steur, L., Divine, D., Gerland, S., Hansen, E., & Kwok, R. (2020). Arctic sea ice volume export through fram strait from 1992 to 2014. *Journal of Geophysical Research: Oceans*, 125(6), e2019JC016039. <https://doi.org/10.1029/2019jc016039>
- Spreen, G., Kwok, R., & Menemenlis, D. (2011). Trends in arctic sea ice drift and role of wind forcing: 1992–2009. *Geophysical Research Letters*, 38(19), L19501. <https://doi.org/10.1029/2011gl048970>
- Sun, S., & Eisenman, I. (2021). Observed Antarctic sea ice expansion reproduced in a climate model after correcting biases in sea ice drift velocity. *Nature Communications*, 12(1), 1–6. <https://doi.org/10.1038/s41467-021-21412-z>

- Taylor, K. E., Stouffer, R. J., & Meehl, G. A. (2011). An overview of CMIP5 and the experiment design. *Bulletin of the American Meteorological Society*, 93(4), 485–498. <https://doi.org/10.1175/BAMS-D-11-00094.1>
- Thorndike, A. S. (1992). A toy model linking atmospheric thermal radiation and sea ice growth. *Journal of Geophysical Research*, 97, 9401–9410. <https://doi.org/10.1029/92jc00695>
- Tschudi, M., Meier, W. N., Stewart, J. S., Fowler, C., & Maslanik, J. (2019). *Polar pathfinder daily 25 km ease-grid sea ice motion vectors, version 4. NASA National Snow and Ice Data*. Boulder, Colorado USA: Center Distributed Active Archive Center. <https://doi.org/10.5067/INAWUW07QH7B>
- Turner, J., Comiso, J. C., Marshall, G. J., Lachlan-Cope, T. A., Bracegirdle, T., Maksym, T., et al. (2009). Non-annular atmospheric circulation change induced by stratospheric ozone depletion and its role in the recent increase of Antarctic sea ice extent. *Geophysical Research Letters*, 36, L08502. <https://doi.org/10.1029/2009GL037524>
- Turner, J., Hosking, J. S., Marshall, G. J., Phillips, T., & Bracegirdle, T. J. (2016). Antarctic sea ice increase consistent with intrinsic variability of the Amundsen Sea low. *Climate Dynamics*, 46(7–8), 2391–2402. <https://doi.org/10.1007/s00382-015-2708-9>
- Wagner, T. J. W., & Eisenman, I. (2015). How climate model complexity influences sea ice stability. *Journal of Climate*, 28(10), 3998–4014. <https://doi.org/10.1175/JCLI-D-14-00654.1>
- Wettstein, J. J., & Deser, C. (2014). Internal variability in projections of twenty-first-century Arctic sea ice loss: Role of the large-scale atmospheric circulation. *Journal of Climate*, 27(2), 527–550. <https://doi.org/10.1175/JCLI-D-12-00839.1>
- Zhang, J. L., & Rothrock, D. A. (2003). Modeling global sea ice with a thickness and enthalpy distribution model in generalized curvilinear coordinates. *Monthly Weather Review*, 131(5), 845–861. [https://doi.org/10.1175/1520-0493\(2003\)131<0845:mgsiwa>2.0.co;2](https://doi.org/10.1175/1520-0493(2003)131<0845:mgsiwa>2.0.co;2)

Supporting Information for “How sea ice drift influences sea ice area and volume”

T. J. W. Wagner ^{1,2}, I. Eisenman ³, H. C. Mason ^{4,2}

¹Department of Atmospheric and Oceanic Sciences, University of Wisconsin-Madison, WI

²Department of Physics and Physical Oceanography, University of North Carolina Wilmington, NC

³Scripps Institution of Oceanography, University of California San Diego, CA

⁴Courant Institute of Mathematical Sciences, New York University, NY

Contents of this file

- Text S1 – Model Equations
- Table S1
- Figures S1 to S7

Text S1 – Model Equations

The model used here is identical to that in WE15 (Wagner & Eisenman, 2015), aside from the addition of meridional ice drift as discussed in the main text. The model can be written in terms of a single partial differential equation (eq 1 in the main text):

$$\frac{\partial E}{\partial t} = \underbrace{aS}_{\text{solar}} - \underbrace{(A + BT)}_{\text{OLR}} + \underbrace{D\nabla_x^2 T}_{\text{transport}} + \underbrace{F_b}_{\text{ocean heating}} + \underbrace{F}_{\text{climate forcing}} + \underbrace{M\mathcal{H}(-E)}_{\text{ice motion}}, \quad (1)$$

where the planetary co-albedo is written as

$$a(x, E) = \begin{cases} a_0 - a_2 x^2 & E > 0 \quad (\text{open water}), \\ a_i & E < 0 \quad (\text{ice}), \end{cases} \quad (S2)$$

and the time-varying insolation as

$$S(t, x) = S_0 - S_1 \cos(\omega t) x - S_2 x^2. \quad (S3)$$

Here, due to converging meridians on a spherical earth, meridional diffusion takes the form

$$D\nabla^2 T = D \frac{\partial}{\partial x} \left[(1 - x^2) \frac{\partial T}{\partial x} \right]. \quad (S4)$$

Surface temperature is computed for the following three regimes:

$$T = \begin{cases} T_m + E/c_w & E > 0 & (\text{open water}), \\ T_m & E < 0, \quad T_0 > T_m & (\text{melting ice}), \\ T_0 & E < 0, \quad T_0 < T_m & (\text{freezing ice}), \end{cases} \quad (S5)$$

where T_0 is obtained by balancing the surface energy fluxes and solving

$$k(T_m - T_0)/h = -aS + A + B(T - T_m) - D\nabla^2 T - F. \quad (S6)$$

More detail on the derivation of these equations and implied assumptions can be found in WE15. The default parameter values are provided in Table S1.

	Description	Value	Unit
D	diffusivity for heat transport	0.6	$\text{Wm}^{-2}\text{K}^{-1}$
A	OLR when $T = T_m$	193	Wm^{-2}
B	OLR temperature dependence	2.1	$\text{Wm}^{-2}\text{K}^{-1}$
c_w	ocean mixed layer heat capacity	9.8	$\text{Wyr m}^{-2}\text{K}^{-1}$
S_0	insolation at equator	420	Wm^{-2}
S_1	insolation seasonal dependence	338	Wm^{-2}
S_2	insolation spatial dependence	240	Wm^{-2}
a_0	ice-free co-albedo at equator	0.7	-
a_2	ice-free co-albedo spatial dependence	0.1	-
a_i	co-albedo where there is sea ice	0.4	-
F_b	heat flux from ocean below	4	Wm^{-2}
k	sea ice thermal conductivity	2	$\text{Wm}^{-1}\text{K}^{-1}$
L_f	sea ice latent heat of fusion	9.5	Wyr m^{-3}
T_m	melting temperature	0	$^{\circ}\text{C}$
c_g	ghost layer heat capacity	0.098	$\text{Wyr m}^{-2}\text{K}^{-1}$
τ_g	ghost layer coupling timescale	1×10^{-5}	yr
F	radiative forcing	0 (varies)	Wm^{-2}
v	meridional ice drift speed	0 (varies)	m s^{-1}

Table S1. Model Default Parameter Values. Values for all parameters except v are as in Wagner and Eisenman (2015).

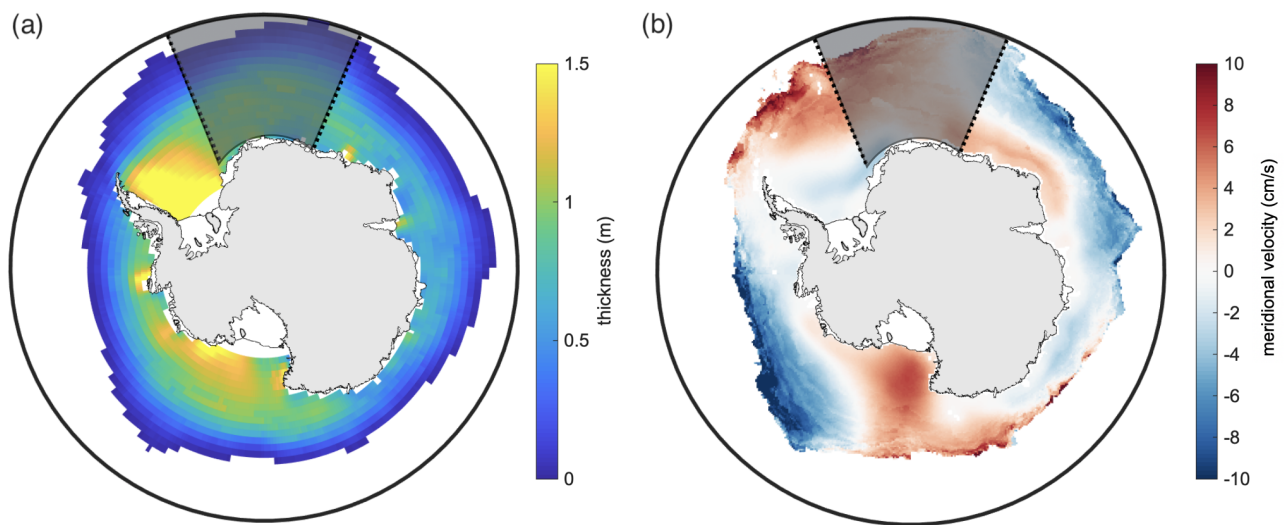


Figure S1. (a) Annual mean Antarctic sea ice thickness from the GIOMAS state estimate (Zhang & Rothrock, 2003). The Dronning Maud Land section is highlighted in gray. (b) Annual mean meridional sea ice velocity from Tschudi et al. (2019).

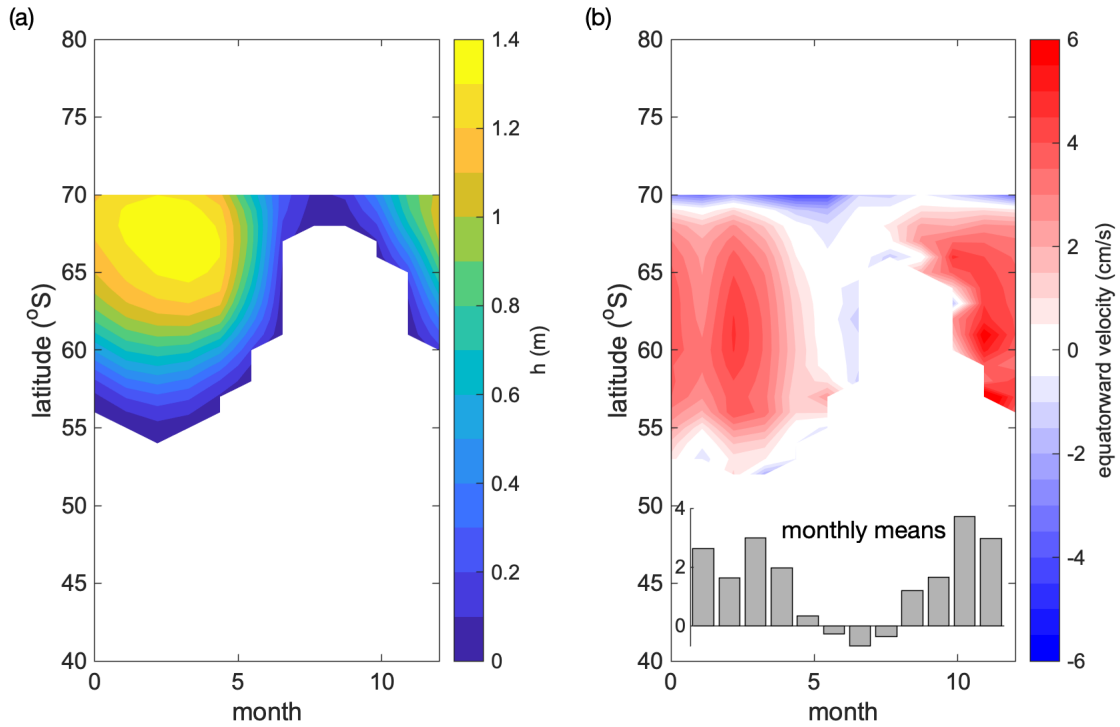


Figure S2. (a) Climatological zonally averaged ice thickness in Dronning Maud Land from GIOMAS. (b) Climatological zonally averaged equatorward velocities in Dronning Maud Land from Tschudi et al. (2019). Inset: Monthly mean spatially-averaged equatorward velocities in Dronning Maud Land, used to force model for Figure S3b .

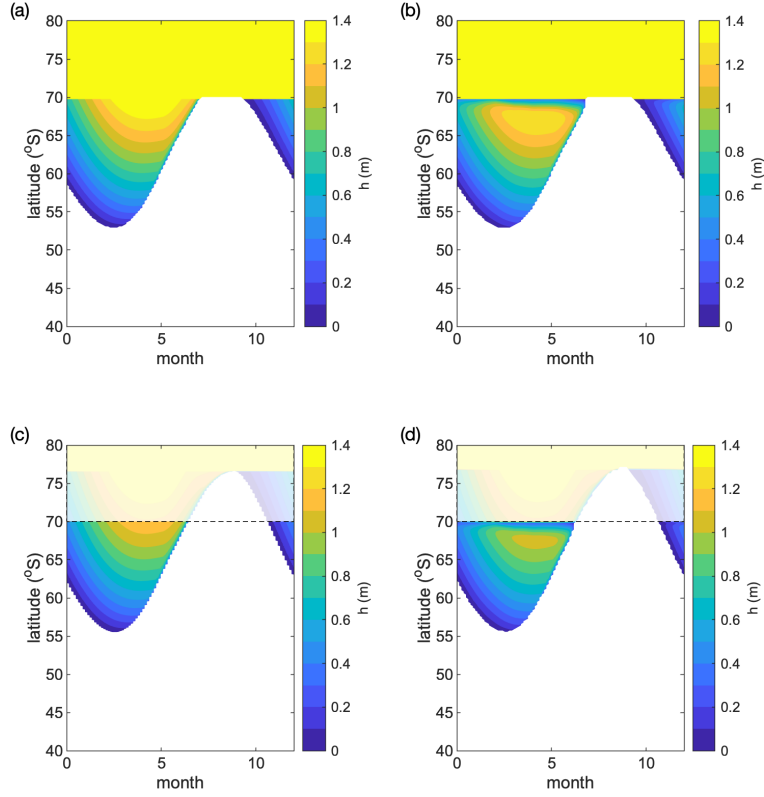


Figure S3. (a) Model simulation with idealized Antarctic landmass and zero ice motion. Here, the landmass is represented by specifying $h = 100$ m poleward of $\theta = 70^\circ\text{S}$. (b) As in (a) but with ice motion prescribed, using equatorward velocities as shown in the inset of Figure S2b. It should be noted that the large Stefan Number approximation (used to motivate constant vertical heat flux in the sea ice) does not hold for such thick ice since in this case sensible heat changes in the ice would no longer be small compared to latent heat changes. Relatedly, annual variations in surface temperature would realistically only penetrate the thick ice to a depth of a few meters. However, we find that our results are rather insensitive to the exact representation of the idealized landmass and even simulations with the default configuration produce qualitatively similar results in the latitudes of interest when forced with the velocities used in panels (a) and (b), as shown in panels c (for zero ice motion) and d (for ice motion as in panel b, acting only on ice in the region $\theta < 70^\circ\text{S}$). White shading is added to draw the focus on the region $\theta < 70^\circ\text{S}$. Note that panel c is identical to Fig 2b, except for the range of latitudes and contours.

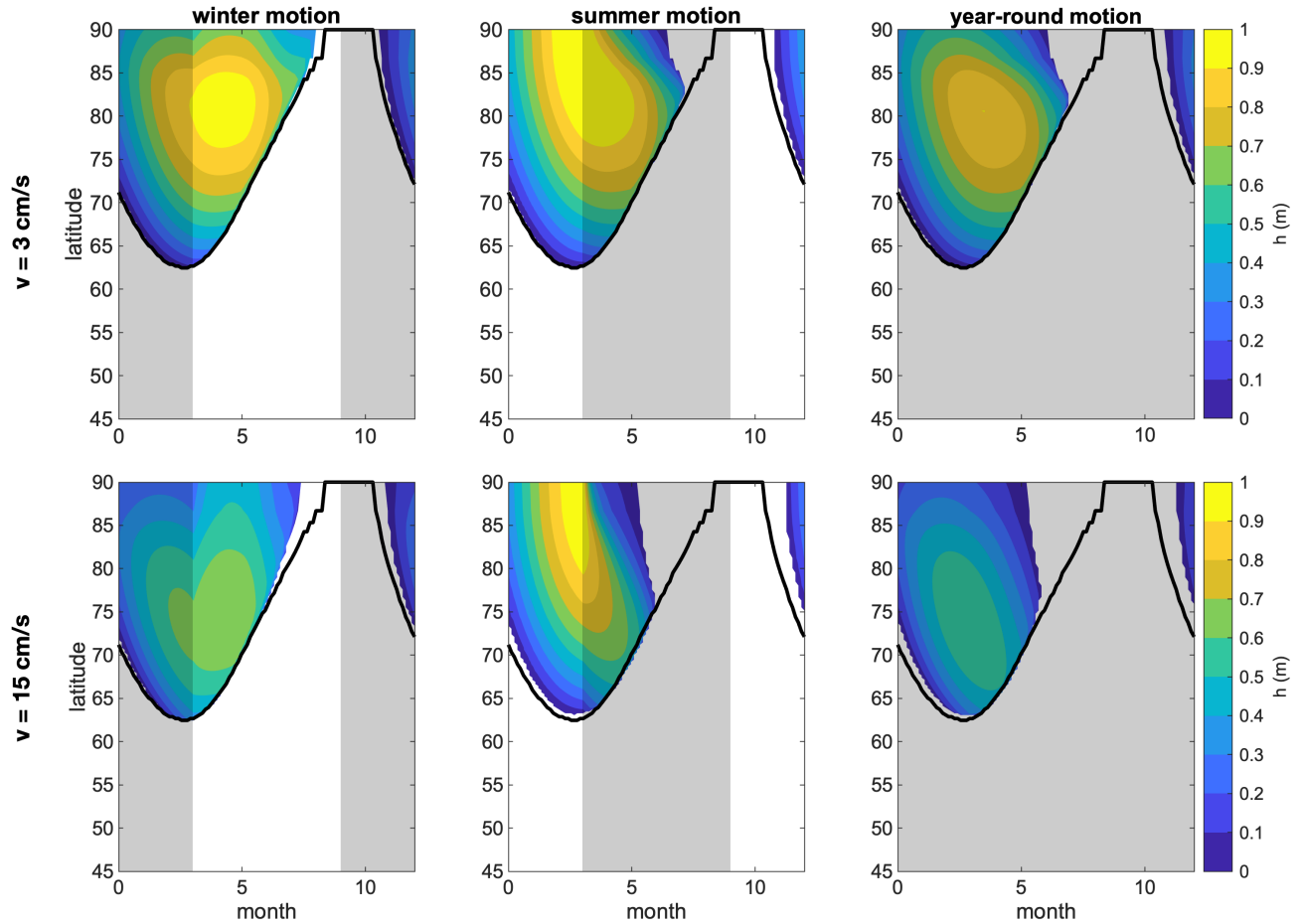


Figure S4. Seasonal cycle of sea ice thickness, as in Figure 2 of the main text, but for climate forcing $F = 4 \text{ W m}^{-2}$. Here, again, $v = 3 \text{ cm s}^{-1}$ (top row) and $v = 15 \text{ cm s}^{-1}$ (bottom row). The first column represents motion during 6 months of ice advance (“winter”), the second column shows motion during 6 months of ice retreat (“summer”), and the third column gives the case of motion throughout the year. The gray shaded regions in each panel depict the period in which ice is moving.

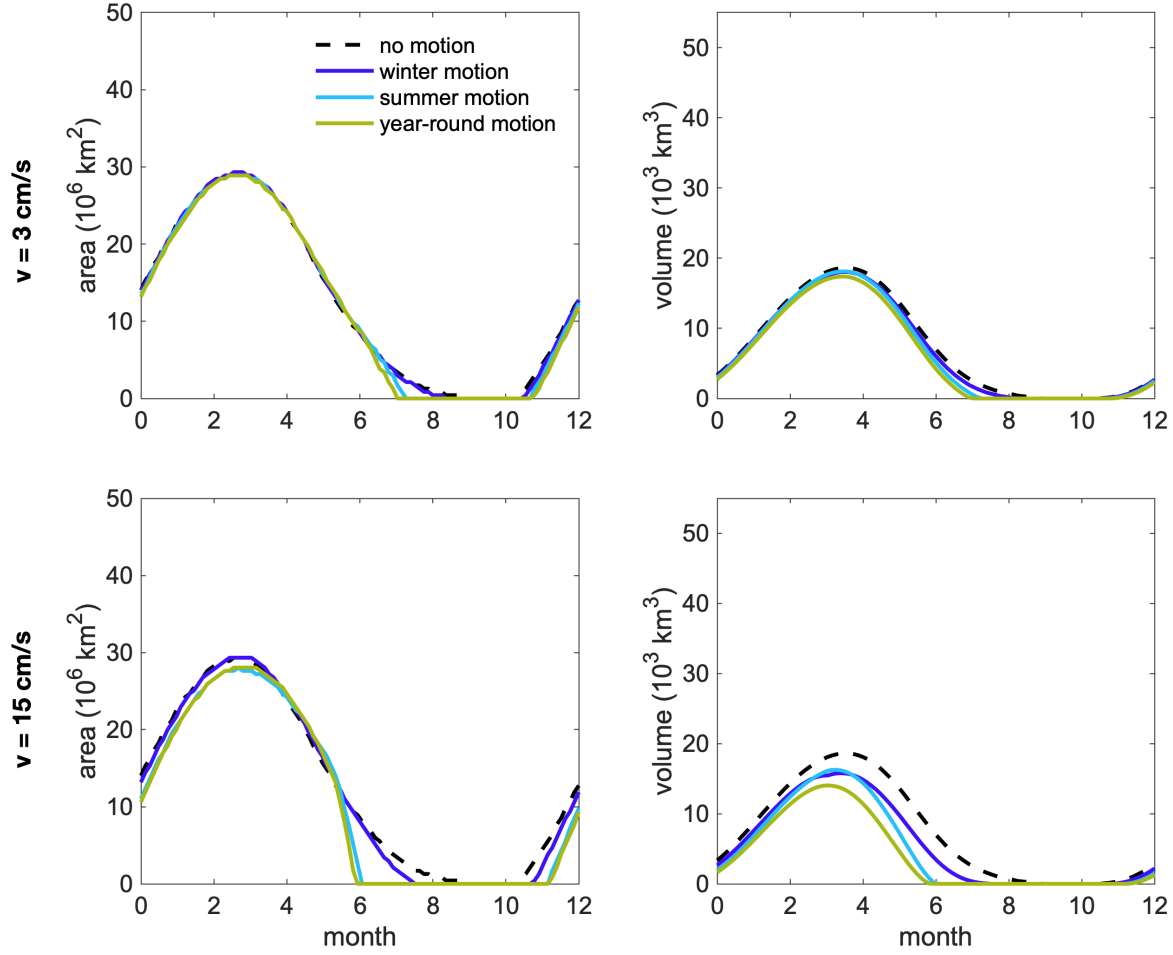


Figure S5. Steady-state sea ice seasonal cycle in response to ice drift during different periods of the year, as in Figure 3 of the main text, but for climate forcing $F = 4 \text{ W m}^{-2}$. (a,c) Ice area as a function of time of year for the scenarios of no motion (black dashed), winter-only motion (dark blue), summer-only motion (light blue), and year-round motion (green). (b,d) Same as panels a and c, but for ice volume. The top row corresponds to drift speed $v = 3 \text{ cm s}^{-1}$, and the bottom row to $v = 15 \text{ cm s}^{-1}$, as in Figure S4.

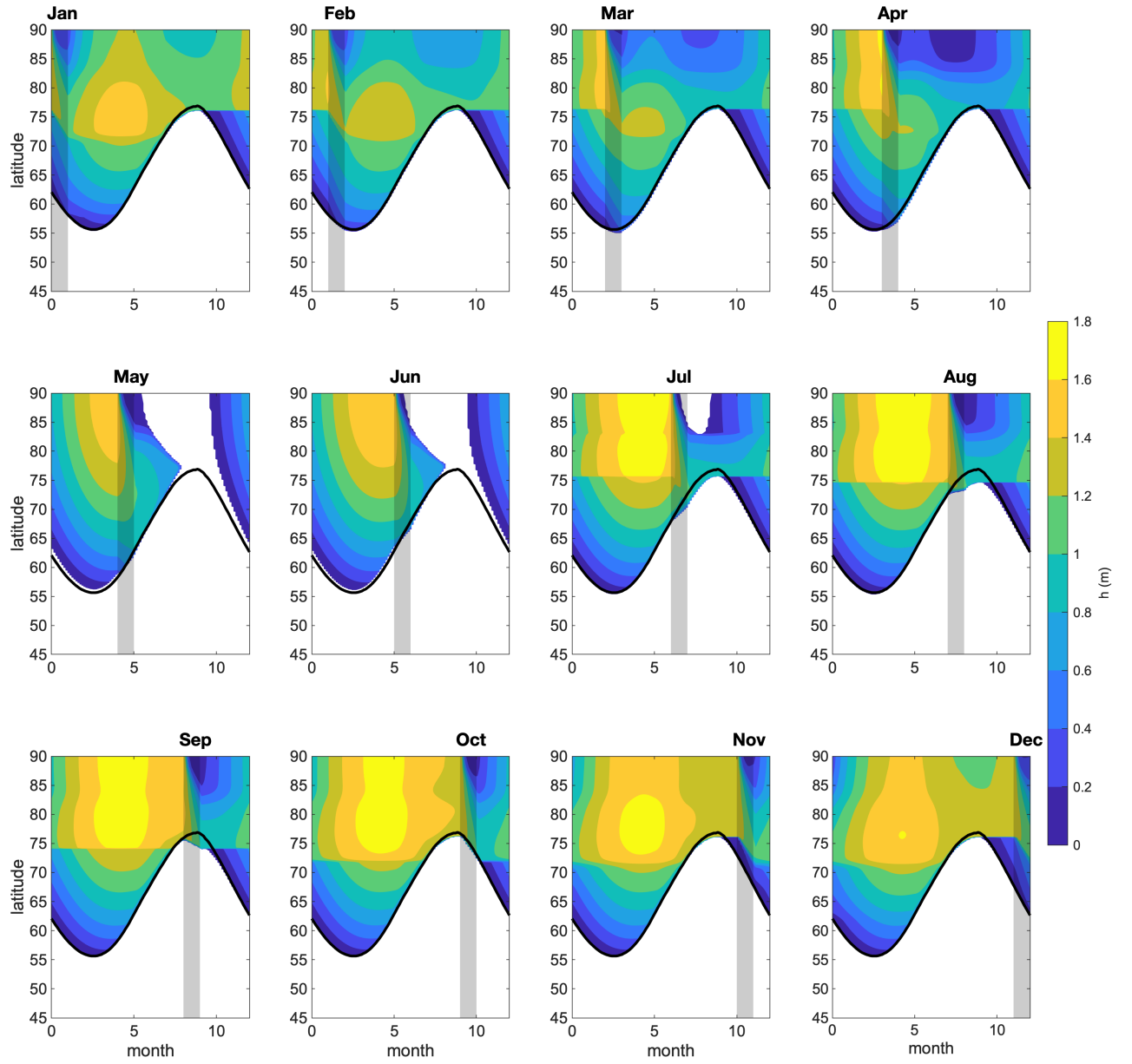


Figure S6. Steady-state sea ice seasonal cycle in response to ice drift during different periods of the year, as in Figure 2 of the main text, but for single-month motion, rather than seasonal or year-round. Here, $F = 0$ and $v = 15 \text{ cm s}^{-1}$.

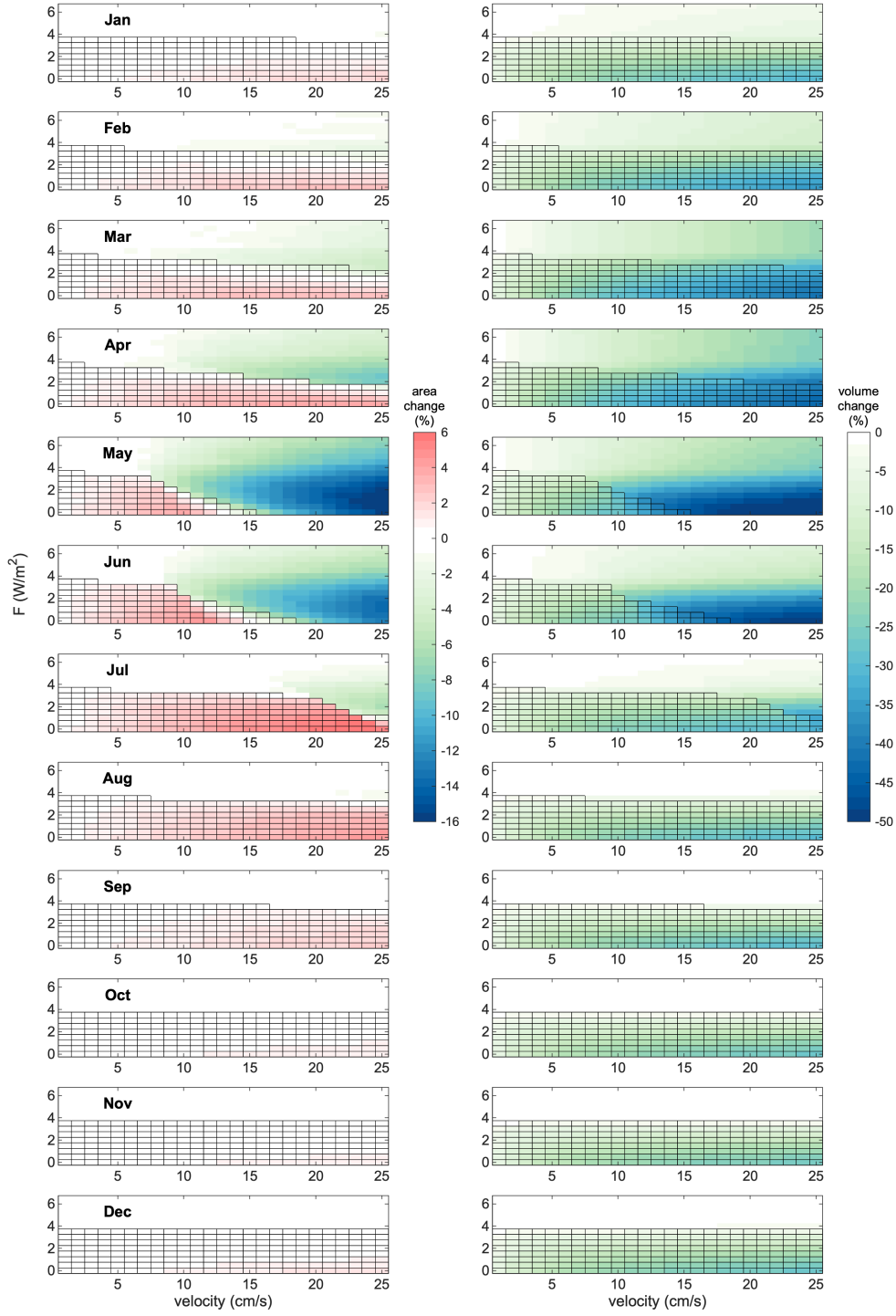


Figure S7. Annual mean response of the sea ice cover to equatorward ice drift, for different climate forcings F (vertical axes) and drift speeds v (horizontal axes), as in Fig 4 of the main text, but for single-month motion, rather than seasonal or year-round.

References

- Tschudi, M., Meier, W. N., Stewart, J. S., Fowler, C., & Maslanik, J. (2019). Polar pathfinder daily 25 km ease-grid sea ice motion vectors, version 4. *NASA National Snow and Ice Data Center Distributed Active Archive Center, Boulder, Colorado USA*, accessed February 2021. doi: 10.5067/INAWUWO7QH7B
- Wagner, T. J. W., & Eisenman, I. (2015). How climate model complexity influences sea ice stability. *J. Climate*, 28(10), 3998–4014. doi: 10.1175/JCLI-D-14-00654.1
- Zhang, J. L., & Rothrock, D. A. (2003). Modeling global sea ice with a thickness and enthalpy distribution model in generalized curvilinear coordinates. *Monthly Weather Rev.*, 131(5), 845–861.